Tsunami source imaging using adjoint-state inversion of data from ocean bottom pressure gauges

Saeed Y. Mohanna[1] (saeedmohanna@g.ucla.edu); Yuqing Xie[1] (xieyq@ucla.edu); Lingsen Meng[1] (meng@epss.ucla.edu)

[1]Earth, Planetary and Space Sciences, University of California, Los Angeles, CA, USA.

Abstract

Current frameworks for issuing rapid tsunami warnings rely on point-source models that do not consider slip distribution or the rupture area of the corresponding earthquakes and thus can be inaccurate in the immediate aftermath of an event, leading to inaccurate wave height and wave arrival time predictions. In response to the underestimation of tsunami wave height during the 2011 Tohoku tsunami, the Japanese Meteorological Agency (JMA) constructed the Seafloor Observation Network for Earthquakes and Tsunamis along the Japan Trench (S-net), a dense data network of 150 ocean bottom pressure gauges (OBPG) to avoid reliance on accurate earthquake models in order to issue a tsunami warning. To take advantage of S-net, our group developed an algorithm that inverts OBPG data using the adjoint-state method to yield the tsunami source directly, eliminating reliance on accurate earthquake models. We tested the adjoint-state method on synthetic waveforms and OBPG data of the 2011 M_w 9.0 Tohoku and 2016 M_w 6.9 Off-Fukushima earthquakes, respectively. The results from these tests show that this method can yield wave-height predictions with an average accuracy of 93% and 78% using the first 5 and 25 minutes of the synthetic and observed OBPG data, respectively. We also sought to investigate whether our method can invert for an earthquake's rupture speed and consider its effect on our ability to predict tsunami waves. Most tsunami simulations assume a time-independent source model, where the sea-floor deforms all at once. However, this can be inaccurate for large earthquakes with slow rupture speed leading to propagation of the deformation over time, creating a time-dependent source. Consequently, we first tested our method using synthetic data of a tsunami sourced near the region of the 2011 Tohoku event, in which we mimic a scenario where a rupture is triggered 200 s after the origin time, as suggested by previous studies. Our results when using 5-10 mins of synthetic OBPG data yielded wave-height predictions that were close to that of the synthetic data, with variance reductions converging to 0.95 after 7 iterations of the inversion in most cases.

Motivation

Tsunami warnings have been inaccurate in their wave height predictions due to reliance on accurate seismic models. The prime example of this is the 2011 Tohoku tsunami, where tsunami warnings underestimated wave-heights as a result of underestimating the earthquake magnitude. As a result, JMA constructed S-net (Figure 1) in order to monitor the deformation of the seafloor directly, without relying on accurate earthquake models. Our group has taken advantage of this network by developing a method that inverts OBPG data using the adjoint-state method to yield the tsunami source's initial water elevation and wave height predictions directly, thus eliminating the reliance on an accurate earthquake model (Zhou et al., 2019) and reducing the computation time that would otherwise be spent calculating Green's functions for every grid in a densely gridded source region. In order to test the effectiveness of this method, we apply it to synthetic and real data of S-net's OBPGs.

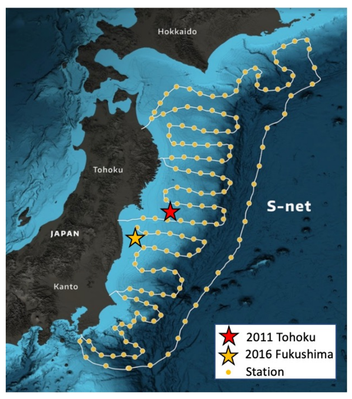

Figure 1: Map showing the configuration of S-net stations along the Japan Trench in addition to the epicenters of the two earthquakes of interest. White line traces the cable link between stations. Modified from University of Washington tsunami early warning website (www.cev.washington.edu)

Method

The adjoint-state method incorporates a technique known as time-reversal imaging (TRI; Hossen et al., 2015). It is a method that involves reversing waveforms from all recording stations in time and propagating them back to the origin time of the event of interest (Figure 2). If we have a dense network of stations with sufficient azimuthal coverage, then the source region of the model can be constrained relatively accurately.

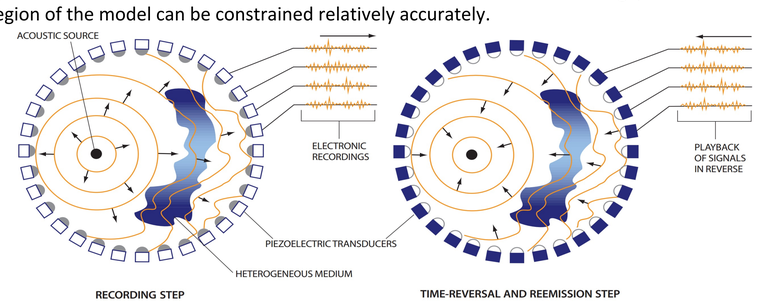

Figure 2: Illustration of the concept of time-reversal imaging when applied to an acoustic source (Fink, 1999).

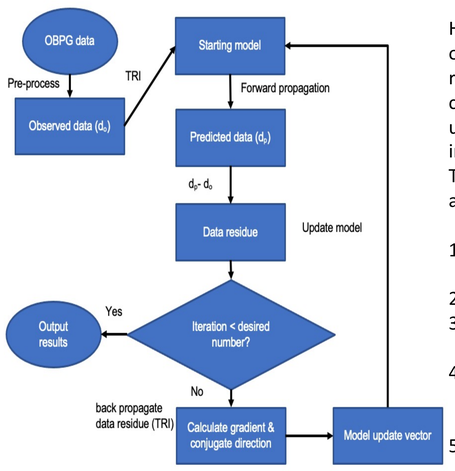

Figure 3: The workflow of the adjoint-state tsunami source inversion method (modified from Zhou et al., 2019).

For the time-dependent inversion, the only change we make in our inversion process is adding a step where we back-propagate using TRI to the origin time of the tsunami -200 seconds. And then the resulting adjoint wavefield is used to update the outputted model at t=200 s.

However, the wave height predictions obtained after forward propagating the resulting source model to station locations can be inaccurate. Consequently, we only use this technique because it offers a good initial guess for the desired source model. The steps of our inversion (Figure 3) are as follows:

1) Pre-process OBPG data and obtain bathymetry data
2) Perform TRI to obtain starting model
3) Forward propagate starting model to station locations
4) Calculate the data residue and check if we have reached the desired number of iterations to output the results
5) If not, then back propagate the data residue using TRI
6) Calculate the adjoint wavefield and use the conjugate gradient direction to update the model
7) Repeat steps 3-6 until you reach the desired amount of iterations/data residue converges.

Data

For most of our simulations, we assume a time-independent source in which all the seismic slip occurs at the origin time. However, this assumption can be inaccurate for events such as the 2015 M_w 8.3 Illapel earthquake, where two major peaks are seen in the source-time function. So, in order to explore the capabilities of our method, we also test its performance on simple time-dependent synthetic data of the 2011 event.

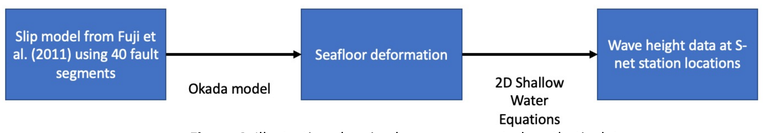

Figure 4: Illustration showing how we generated synthetic data.

To generate synthetic data of the 2011 tsunami (assuming a time-independent source), we follow the scheme in figure 4. We assume that the fault segments all slip at the same time. We use the Parallel Cornell Multi-grid Coupled Tsunami modeling package (PCOMCOT) for all forward propagations of the seafloor deformation to station locations.

The synthetic waveforms consist of the coseismic deformation of the seafloor and the change of the water column height over time at a given point (figure 5d black lines). However, the OBPGs record the change of pressure, which is only related to the water column height above the station. This means the coseismic deformation affects the recordings at near-field stations. To mimic the real case for the recording of the S-net stations, we remove the coseismic deformation by shifting the synthetic waveforms so that the amplitudes of the tsunami waves are 0 after the duration of the earthquake to obtain the water column height change (figure 5b blue lines). In a real scenario, we would take the average amplitude of the blue lines in the last minute of the chosen time window and then add this value to the change of water column height to obtain an estimate of the true water elevation (figure 5b red-dashed lines).

Figure 5: Illustration of correction for coseismic effect. **(a)-(c)** show water elevation (black arrow/lines) and pressure-derived water column height (blue arrows/lines) before (a), during (b) and after the tsunami wave passes over stations (yellow triangles). Water is blue color and seafloor is in orange. **(d)** shows sample waveforms from stations near (left and middle) and far (right) from the principal-slip region. Red-dashed line shows correction result using the method described.

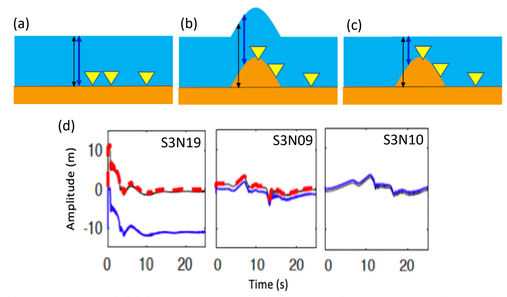

Assuming a time-dependent inversion for the 2011 event, we generate simple gaussian slip models that slip t=0 and t=200 s (Figure 6 top panel).

For the 2016 Off-Fukushima event, we use data from 125 stations as the remaining 25 stations were not yet operational. Since stations close to the source are contaminated by non-tsunami signals, we first low-pass filter (100 s) to remove seismic effects. Then, the instrumentation-attributed steps in the data are removed if the time derivative at a particular time is greater than 0.0005 m/s. Finally, a high-pass filter (1000 s) was applied to remove tidal effects.

Synthetic tests

For the time-dependent source, the initial water elevation (figure 6) at all time slices matched the synthetic model well. In order to evaluate the prediction accuracy of our model, we calculated the variance reduction (VR) between observed and predicted waveforms for various iterations and time windows (figure 9).

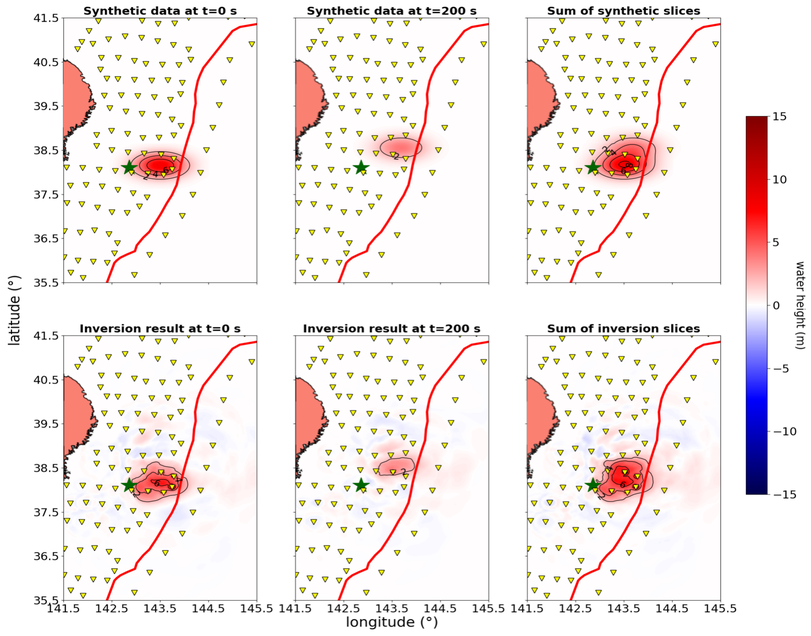

Figure 6: Maps showing initial water elevation for the 2011 Tohoku tsunami assuming simple pulse sources that slip at two different times. The inversion results are after 20 iterations using 9-min waveforms. The rightmost panels show the sum of the two sources.

VRs converged to ~0.95 after 7 iterations for most waveform windows (figure 9c). This encourages to attempt inversions with more complicated time-dependent data in order to invert for an earthquake's rupture speed.

Our outputted initial water elevation (figure 7) of the time-independent source for the 2011 event matches very well with the synthetic data after just 10 iterations. The inversion took ~80 seconds to run when using 16 CPU cores and bathymetry with a resolution of 90 arc seconds.

VR analysis shows that allowing the tsunami source to propagate for 8 mins yields a higher VR after convergence compared to other time windows. Choosing too short a time window means the tsunami waves do not have time to propagate to many stations, thus limiting the ability of the inversion to accurately model the coseismic deformation. Choosing too long a time window can introduce reflections off coastlines, which leads to unwanted artifacts and lower VR values at stations in the artifact regions. Using the results with 5-min waveforms, we obtain an average accuracy for wave height predictions of 93%.

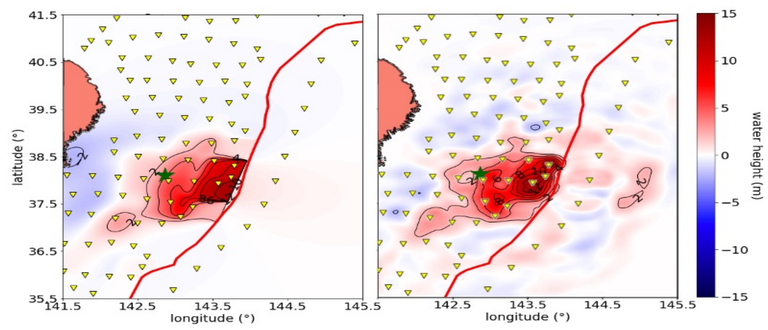

Figure 7: Maps of our region of interest showing initial water elevation for the 2011 Tohoku tsunami assuming all subfaults slip at the same time. Left panel shows synthetic data, and the right panel shows results of our inversion after 10 iterations using 8-min waveforms. The contours show water subsidence (blue) and uplift (red) levels at intervals of 2 m, with the interval at 0 m being omitted for clarity. Inverted yellow triangles represent location of S-net stations. Honshu island shown in salmon. Green star shows the mainshock's epicenter. Red line traces the Japan Trench.

Application to the 2016 Off-Fukushima tsunami

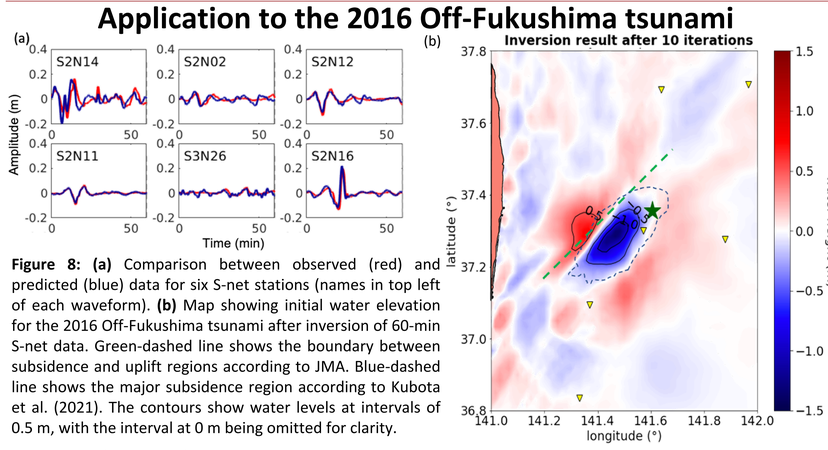

Figure 8: (a) Comparison between observed (red) and predicted (blue) data for six S-net stations (names in top left of each waveform). **(b)** Map showing initial water elevation for the 2016 Off-Fukushima tsunami after inversion of 60-min S-net data. Green-dashed line shows the boundary between subsidence and uplift regions according to JMA. Blue-dashed line shows the major subsidence region according to Kubota et al. (2021). The contours show water levels at intervals of 0.5 m, with the interval at 0 m being omitted for clarity.

The result (figure 8b) matches closely with the major subsidence region obtained by Kubota et al. (2021) as well as the boundary between uplift and subsidence according to JMA. Using the results with 25-min waveforms, we obtain an average accuracy for wave height predictions of 78% . VRs were highest when using waveforms that were 40-60 mins in length (figure 8b).

Discussion

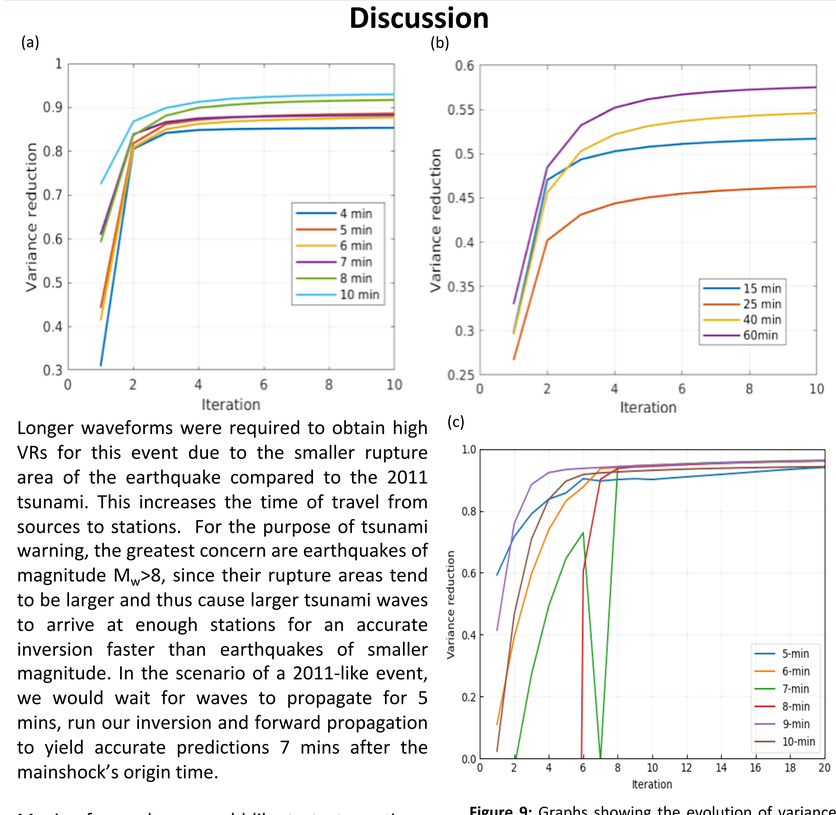

Longer waveforms were required to obtain high VRs for this event due to the smaller rupture area of the earthquake compared to the 2011 tsunami. This increases the time of travel from sources to stations. For the purpose of tsunami warning, the greatest concern are earthquakes of magnitude M_w>8, since their rupture areas tend to be larger and thus cause larger tsunami waves to arrive at enough stations for an accurate inversion faster than earthquakes of smaller magnitude. In the scenario of a 2011-like event, we would wait for waves to propagate for 5 mins, run our inversion and forward propagation to yield accurate predictions 7 mins after the mainshock's origin time.

Moving forward, we would like to test our time-dependent inversion on more complex scenarios such as multiple ruptures occurring at more than two time slices. Once this is achieved, we can begin to conduct optimization analysis at high-tsunami-risk locations for the number of stations and configuration that yields accurate inversion results using the adjoint-state method.

Figure 9: Graphs showing the evolution of variance reduction between observed and predicted waveforms with increasing iterations using data of various time windows. (a) corresponds to the synthetic time-independent data for the 2011 Tohoku tsunami, (b) corresponds to the S-net data for the 2016 Off-Fukushima earthquake, and (c) corresponds to the synthetic time-dependent data for the 2011 Tohoku tsunami.

References

Hossen, M. J., Cummins, P. R., Roberts, S. G., & Allgeyer, S. (2015). Time reversal imaging of the Tsunami Source. *Pure and Applied Geophysics*, *172*(3-4), 969–984. https://doi.org/10.1007/s00024-014-1014-5

Kubota, T., Kubo, H., Yoshida, K., Chikasada, N. Y., Suzuki, W., Nakamura, T., & Tsushima, H. (2021). Improving the constraint on the M_w 7.1 2016 Off-Fukushima shallow normal-faulting earthquake with the high azimuthal coverage tsunami data from the s-net wide and dense network: Implication for the stress regime in the Tohoku overriding plate. *Journal of Geophysical Research: Solid Earth*, *126*(10). https://doi.org/10.1029/2021jb022223

Zhou, T., Meng, L., Xie, Y., & Han, J. (2019). An adjoint-state full-waveform tsunami source inversion method and its application to the 2014 Chile-Iquique tsunami event. *Journal of Geophysical Research: Solid Earth*, *124*(7), 6737–6750. https://doi.org/10.1029/2018jb016678

Acknowledgements

This work is supported by the National Science Foundation's award number 1848486 and by the Leon and Joanne V.C. Knopoff Fund.